

## Article

# Effect of One Sulfate-Reducing Bacterium SRB-Z Isolated from Pearl River on the Corrosion Behavior of Q235 Carbon Steel

Hong Qi <sup>1</sup>, Qingshan Shi <sup>1</sup>, Ruqun Peng <sup>1</sup>, Tingli Sun <sup>1</sup>, Zheng Zhang <sup>2,\*</sup>, Liangqiu Li <sup>1,\*</sup> and Xiaobao Xie <sup>1,\*</sup>

<sup>1</sup> Key Laboratory of Agricultural Microbiomics and Precision Application (MARA), Guangdong Provincial Key Laboratory of Microbial Culture Collection and Application, Key Laboratory of Agricultural Microbiome (MARA), State Key Laboratory of Applied Microbiology Southern China, Institute of Microbiology, Guangdong Academy of Sciences, Guangzhou 510070, China

<sup>2</sup> Guangdong Provincial Key Laboratory of Electronic Information Products Reliability Technology, Guangzhou 510610, China

\* Correspondence: zhangzh@ceprei.com (Z.Z.); liliangqiu@gdim.cn (L.L.); xiexb@gdim.cn (X.X.); Tel.: +86-13825026868 (Z.Z.); +86-13543466160 (L.L.); +86-13660168677 (X.X.)

**Abstract:** Sulfate-reducing bacteria (SRB) have long been reported to participate in metal corrosion processes in anoxic environments. However, existing theories still need enrichment by identifying more corrosive microorganisms and exploring more plausible microbiologically-influenced corrosion pathways. In this study, a strain SRB-Z was isolated from the Pearl River in Guangzhou, and its effect and mechanisms on corrosion of Q235 carbon steel were examined. The biofilms, corrosion products, pits, and corrosion electrochemistry were characterized by SEM, XPS, CLSM, EDS, white light interferometer 3D profilometry, and electrochemical analysis, respectively. The results of this study indicate that SRB-Z could cause serious pitting of Q235 carbon steel. The maximum pit depth reached 54  $\mu\text{m}$  after immersion corrosion for 7 days. Strain SRB-Z promoted the cathodic reaction rate of Q235. The relative analyses revealed that pitting corrosion occurred because of galvanic corrosion caused by the formation of an FeS-SRB/Fe galvanic couple under the synergistic effect of the SRB-Z biofilm and its metabolite ( $\text{H}_2\text{S}$ ) on the Q235 coupon surfaces.

**Keywords:** microbiologically influenced corrosion; isolated sulfate-reducing bacteria; pitting corrosion; FeS-SRB/Fe galvanic couple



**Citation:** Qi, H.; Shi, Q.; Peng, R.; Sun, T.; Zhang, Z.; Li, L.; Xie, X. Effect of One Sulfate-Reducing Bacterium SRB-Z Isolated from Pearl River on the Corrosion Behavior of Q235 Carbon Steel. *Coatings* **2023**, *13*, 478. <https://doi.org/10.3390/coatings13020478>

Academic Editor: Edoardo Proverbio

Received: 18 November 2022

Revised: 15 January 2023

Accepted: 16 February 2023

Published: 20 February 2023



**Copyright:** © 2023 by the authors. Licensee MDPI, Basel, Switzerland. This article is an open access article distributed under the terms and conditions of the Creative Commons Attribution (CC BY) license (<https://creativecommons.org/licenses/by/4.0/>).

## 1. Introduction

Corrosion is a common problem in humid and aqueous environments such as those found in the oil and gas industry, ocean engineering equipment, and water systems [1–3]. Microbiologically-influenced corrosion (MIC) is usually considered when corrosion phenomena cannot be explained by chemical or electrochemical means [4–6]. For example, some unexpected cracks and pitting observed in industrial applications cause leakage and explosions in pipelines, suspected to be induced by bacteria [7–10]. Extensive research has been conducted on MIC. Sulfate-reducing bacteria (SRB) are widespread in nature. They have been widely reported to participate in metal corrosion processes and are considered the main kind of bacteria which induce MIC [11–16]. They use sulfate as an electron acceptor for anaerobic respiration, producing  $\text{H}_2\text{S}$  [17–21]. Usually, SRB induces local corrosion of metal. Presently, two important mechanisms are recognized as being involved in MIC: (1) Chemical microbiologically-influenced corrosion (CMIC), in which the metal is corroded by corrosive compounds such as biogenic  $\text{H}_2\text{S}$  [22,23]; and (2) Electrical microbiologically-influenced corrosion (EMIC), in which SRB directly or indirectly absorbs electrons from metals [24,25]. However, SRB-influenced corrosion is a complicated process, involving the electron transport process and local corrosion with the participation of biofilm, bacteria metabolites, reaction products, and other factors.

To understand SRB-influenced corrosion of steel, the abundance of microorganisms and the distribution of biofilms on steel surfaces should be considered as being of key

importance [26]. Biofilms are recognized as protected and privileged environments for microbial cell communication, survival, and adaptation [27]. They can maintain the activity of SRB for a long time, inducing continuous corrosion of steel. Nevertheless, biofilm is an overall heterogeneous architecture, containing voids, channels, and pores. So, the thickness of the film varies in different locations. The development of biofilm is a continuous and dynamic process. Mature biofilm can detach from the steel surface by active or passive dispersal strategies. The corrosion effect of biofilm on different areas is not the same. In quiescent or low-shear environments, growing biofilms tend to form circular structures, such as ‘mushrooms’ or mounds [28]. In fast-moving water, growing biofilms tend to form filaments. Thus, due to the high activity of cells in SRB-biofilm, the Shielding function of SRB-biofilm, or the characteristic of super-capacitance of SRB-biofilm, the structure of the biofilm will affect corrosion morphology [29,30]. In addition, the featured reaction product ferrous sulfide (FeS) of SRB-induced corrosion also plays an important role in steel MIC. FeS film usually combines with various minerals and organic sediments in an anaerobic corrosion phase and eventually develops into a composite layer structure combining with biofilms over time. The semiconductive FeS deposited on rough metal surfaces plays a central role in the pitting of SRB MIC [31]. In conclusion, SRB MIC is not induced by a single mechanism, and all of the above factors should be taken into account when studying microbial corrosion. Thus, more corrosive microorganisms in nature and possible MIC pathways should be explored and identified to enrich our knowledge of the existing mechanisms.

In the present work, a corrosive SRB strain was isolated from the natural environment and its effect on the corrosion behavior of Q235 carbon steel was investigated. The immersion corrosion test was conducted in both sterile and SRB-inoculated media. The morphology, pit depth, and electrochemical properties of the Q235 carbon steel in each medium were characterized. The role of biofilm and biogenic H<sub>2</sub>S during the corrosion process was investigated and analyzed. The mechanism of pitting corrosion was also proposed.

## 2. Materials and Methods

### 2.1. Isolation, Screening, and Purification of Bacteria Strains

ATCC 1249 medium was used as an enrichment and isolation culture. The composition of the medium is shown in Table 1. To reduce oxygen dissolution in the medium solution, after boiling, the medium was immediately divided into bottles, which were then sealed with a butyl rubber plug and an aluminum cap. The aluminum caps were crimped into place on the plugged bottle. L-cysteine hydrochloride was added to absorb residual oxygen, followed by adding resazurin to indicate the oxygen level. The sulfate-reducing bacterium was isolated from the Pearl River in Guangzhou, China. The isolation, screening, and purification of the strain occurred as follows. First, a water sample was taken from the Pearl River and hung sterile Q235 coupons in 300 mL anaerobic bottles containing 280 mL of as-received Pearl River water for half a month at 37 °C. Then, the coupons were removed and immediately put into another anaerobic bottle containing 280 mL of sterile ATCC medium 1249, and then continuously incubated at 37 °C until the medium in the bottles became black and smelled of rotten eggs. Finally, these media were taken out and spread on a plate incubated at 37 °C for 7 days in an anaerobic workstation (N<sub>2</sub>:H<sub>2</sub>:CO<sub>2</sub> [80:10:10]) (Whitley A35, Don Whitley Science Limited, Bingley, UK). After incubating for 7 days, a single typical black bacterial colony on the plate was chosen and re-streaked onto the blank agar plate, incubated at 37 °C for 7 days in an anaerobic workstation to purify the isolate. The isolate was examined by Gram staining. Then, 16S rRNA gene was amplification and sequence analysed to identify the isolates. Universal primers (27F and 1492R) were used, and the length of the amplicon was found to be 1500 bp. The isolate was able to produce H<sub>2</sub>S, and was confirmed as Gram-negative bacteria. The cells were slightly curved. Executing BLASTN 2.12.0+ against the 16S rRNA database indicated that the 16S rRNA gene sequence of the isolate had the closest relationship with *Desulfovibrio vulgaris* strain

DSM 644, with a sequence homology of 100%, revealing it to be a strain of *Desulfovibrio* sp. This strain was named SRB-Z.

**Table 1.** Composition of ATCC 1249 medium.

| Composition 1                       |          | Composition 3  |          | Composition 2                   |          |
|-------------------------------------|----------|----------------|----------|---------------------------------|----------|
| MgSO <sub>4</sub>                   | 2.0 g    | Sodium Lactate | 3.5 g    | K <sub>2</sub> HPO <sub>4</sub> | 0.5 g    |
| Sodium Citrate                      | 5.0 g    | Yeast Extract  | 1.0 g    | DI water                        | 200.0 mL |
| CaSO <sub>4</sub> ·H <sub>2</sub> O | 1.0 g    | DI water       | 200.0 mL | -                               | -        |
| NH <sub>4</sub> Cl                  | 1.0 g    | -              | -        | -                               | -        |
| DI water                            | 400.0 mL | -              | -        | -                               | -        |
| L-cysteine hydrochloride            | 0.1 g    | -              | -        | -                               | -        |
| resazurin                           | 200 µL   | -              | -        | -                               | -        |

## 2.2. Metal Material and Immersion Corrosion Test

Table 2 displays the basic test conditions. Q235 carbon steel coupons were cut into square shapes (40 × 15 × 2 mm<sup>3</sup>), abraded with 400 and 800 grit sandpaper, sequentially, and then rinsed with acetone, ethanol, and distilled water, sequentially. Before use, the coupons were dry-heated to sterilize (160 °C, 2 h). Three coupons were hung in three 300 mL anaerobic bottles. Each bottle contained 250 mL medium and the experimental group was inoculated with 3 mL SRB-Z seed culture (OD<sub>600</sub>: ~0.600, 10<sup>7</sup> cells mL<sup>-1</sup>). The corrosion test was incubated at 37 °C. Each test was duplicated using three separate bottles. After 7 days, the coupons were removed from the bottles for use. The coupons were weighed using an analytical balance (AUY220, Shimadzu, Kyoto, Japan), with an accuracy of 10<sup>-4</sup> g. Biofilm and corrosion product were removed from the coupons using Clark's solution [32] before weight measurement.

**Table 2.** Test matrix for the SRB-Z influenced corrosion test.

| Parameters       | Conditions                       |
|------------------|----------------------------------|
| Material         | Q235 carbon steel                |
| SRB strain       | <i>Desulfovibrio</i> sp. (SRB-Z) |
| Culture medium   | ATCC medium 1249                 |
| Temperature      | 37 °C                            |
| pH               | 7.2                              |
| Corrosion period | 7 days                           |

## 2.3. Morphology of Biofilm and Pit Measurement

After a 7-day immersion corrosion test, the coupons were removed from the bottles and buried immediately in color-changing silica gel to dry them, and kept for approximately 24 h in the dry anaerobic workstation. After drying, a layer of gold was deposited on the coupon surface to improve conductivity. Then, morphology and chemical composition of the coupon surfaces were detected by a scanning electron microscopy (SEM) instrument (MIRA LMS, TESCAN, CZ) equipped with an energy-dispersive X-ray spectrometer (EDS) (X-MaxN 20, Oxford, UK) and using Thermo Scientific K-Alpha Nexsa (Thermo Fisher Scientific, New York, NY, USA) X-ray photoelectron spectroscopy (XPS). The pit depth of each coupon was obtained using a white light interferometer 3D profilometer (UP-DUAL MODE, Rtec, San Jose, CA, USA). Biofilm and corrosion product were removed from the coupons using Clark's solution before depth measurements after 7-day immersion corrosion. The data obtained from the 3D profilometer were analyzed using Gwyddion-2.52 software.

## 2.4. Electrochemical Corrosion Analysis

Electrochemical tests were performed in an anaerobic corrosion cell with a classical three-electrode system. The working electrode, reference electrode, and counter electrode were the Q235 steel, saturated Ag/AgCl electrode, and platinum mesh, respectively. The sterile and SRB-Z-inoculated media were used as the electrolyte. The cells were incubated at

37 °C. The open circuit potential (OCP), electrochemical impedance spectroscopy (EIS), and potentiodynamic polarization tests were obtained using an electrochemical workstation (CS350, Corrtest, Wuhan, China). The OCP was steady after testing for about 1 h. EIS was performed based on the OCP, and the amplitude was set as 10 mV, the frequencies ranging from 100 kHz to 10 MHz. Potentiodynamic polarization curves were obtained at a scan rate of 1 mV s<sup>-1</sup>. The EIS of the system was tested on the 1st, 2nd, 4th, 7th, and 14th day, and the potentiodynamic polarization curves were tested on the 7th day. The data were analyzed using CS Studio 5. Each test was duplicated using three separate cells, and each cell contained two working electrodes. The EIS test on the 14th day was conducted on the sample without polarization.

### 2.5. H<sub>2</sub>S Measurement

The concentration of H<sub>2</sub>S in the medium was detected using a hydrogen sulfide assay kit (BC2050, Solarbio, Beijing, China). The results showed that the concentration of H<sub>2</sub>S reached approximately 39 mmol L<sup>-1</sup> after a 2-day immersion test in the SRB-Z system, which may affect the corrosion behavior of the Q235 coupon.

## 3. Results

### 3.1. Morphology and Composition of Biofilm and Corrosion Product

The morphologies of the as-prepared Q235 coupon (abraded with 800 grit sandpaper) and the coupons obtained in the sterile medium after immersing for 7 days are displayed in Figure 1a,b. Some sandpaper scratches were found on the as-prepared coupon surface. These scratches deepened uniformly after the immersion corrosion test in the sterile medium. The corrosion product formed in the SRB-Z-inoculated medium demonstrated two classical morphologies. One type of morphology resembles cauliflower and is shown in Figure 1c,e. The cauliflower-like products are distributed locally on the coupon surface. A small amount of SRB was found in these areas. The cauliflower-like products displayed a distinctly thick and loose characteristic. Moreover, some products peeled off during the corrosion period, or the SEM sample preparation process, and the substrate was exposed. The grain boundary of the exposed substrate could be seen clearly (Figure 1g). The other type of morphology resembles an interpenetrating network, as shown in Figure 1d,f. These network-like products were continuously and covered most areas of the coupon (Figure 1d), and many SRB-Z cells are observed in it, as shown in Figure 1f. The network-like morphology character and the emergence of SRB-Z cells indicate that the network-like product was biofilm [7,33]. Under the network-like products, uniform corrosion of the Q235 substrate occurred. The uniform corrosion morphology is shown in Figure 1h. The morphologies demonstrated that, in the SRB-Z-inoculated medium, the sandpaper scratches and the corrosion traces on the Q235 coupon surface are deeper and more significant than in the sterile medium (Figure 1b).

The elemental composition of the cauliflower-like and the network-like product was detected by EDS, as shown in Figure 2. The EDS spectra show that, after the immersion corrosion test, an amount of S and Fe elements emerged in the corrosion product in the SRB-Z-inoculated medium. The concentration of S and Fe in the cauliflower-like product was higher than that in the network-like product. The peak intensity shows that the concentration of O element was significantly less than that of S, suggesting that the main chemical composition was probably FeS<sub>x</sub> but not SO<sub>4</sub><sup>2-</sup>. The concentrations of C, O, and P elements in the network-like product was higher than that in the cauliflower-like corrosion product, and these elements came from the bacteria.

The composition of the corrosion product was further determined by XPS. As shown in the high-resolution C 1s spectrum in Figure 3a, three distinct peaks located at 284.8, 286.2, and 288.3 eV corresponded to C–C–H, C–O (C–N), and peptide bond [34,35], respectively. In the high-resolution Fe 2p spectrum in Figure 3b, three distinct peaks centered at 710.16, 712.13, and 718.39 eV corresponded to FeS<sub>x</sub>, FeS<sub>y</sub> (x > y > 1), and Fe 2p<sub>2/3</sub> sat, respectively [36,37]. In the high-resolution O 1s spectrum, two peaks located at 531.6 and

534.6 eV corresponded to  $\text{SO}_4^{2-}$  ( $\text{SO}_3^{2-}$ ) and organic O, respectively [38,39]. Finally, the high-resolution S 2p spectrum revealed that three peaks centered at 162.3, 163.7, and 164.9 corresponded to  $\text{FeS}_y$ ,  $\text{FeS}_x$  ( $x > y > 1$ ), and S, respectively [40,41]; and the other three peaks centered at 166.7, 168.5, and 169.8 eV corresponded to  $\text{SO}_4^{2-}$  and  $\text{SO}_3^{2-}$  [42]. The results obtained by XPS tests agree with those obtained by EDS.

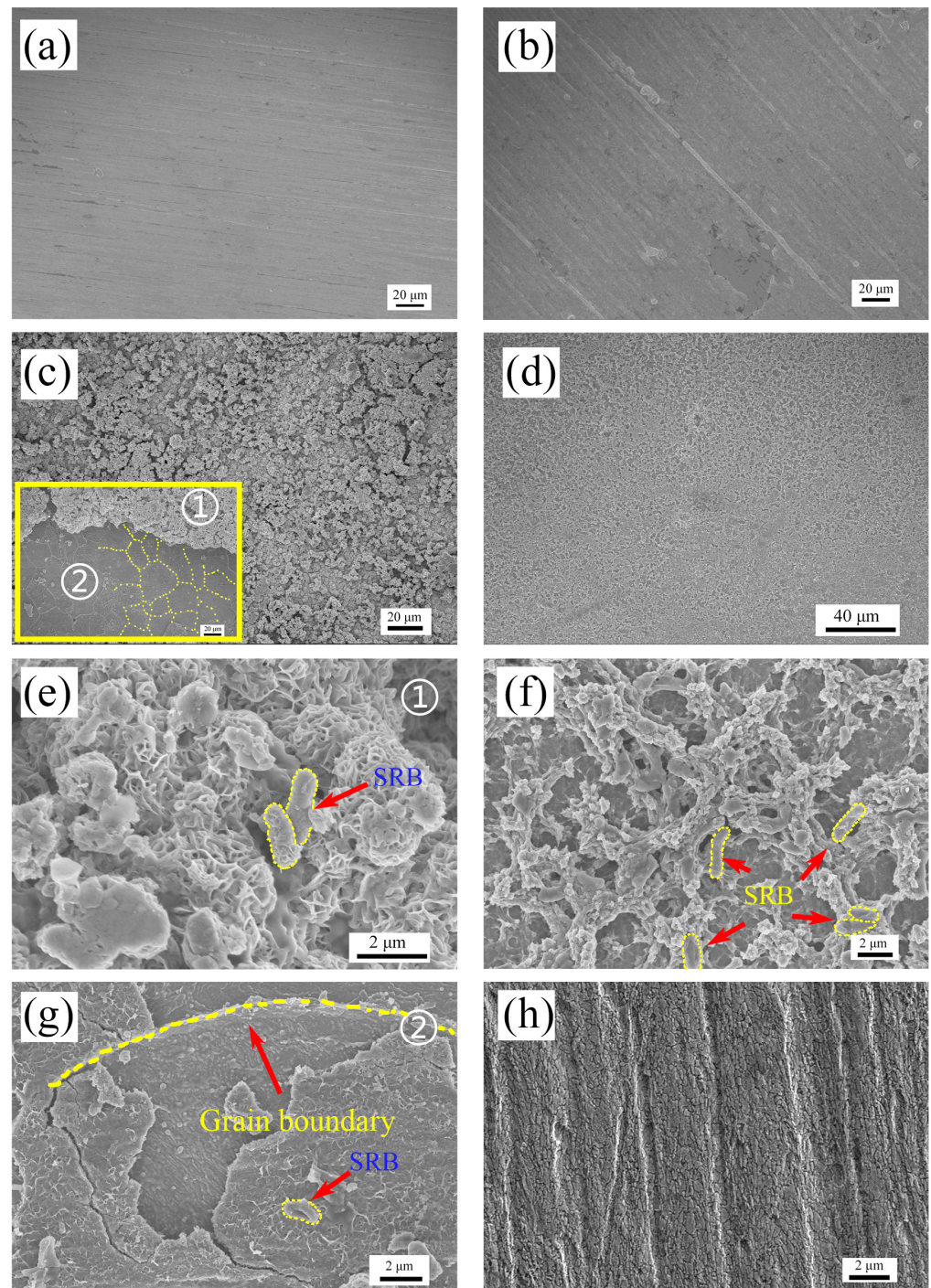


**Figure 1.** The surface morphologies of (a) the original Q235 coupon, (b) the coupon obtained in the sterile medium, and (c–f) the coupon obtained in the SRB-Z-inoculated medium; (e) region ① with cauliflower-like product, (g) region ② the bulgy grain boundary, (d,f) the network-like products, and (h) the corrosion morphology under the network-like product.

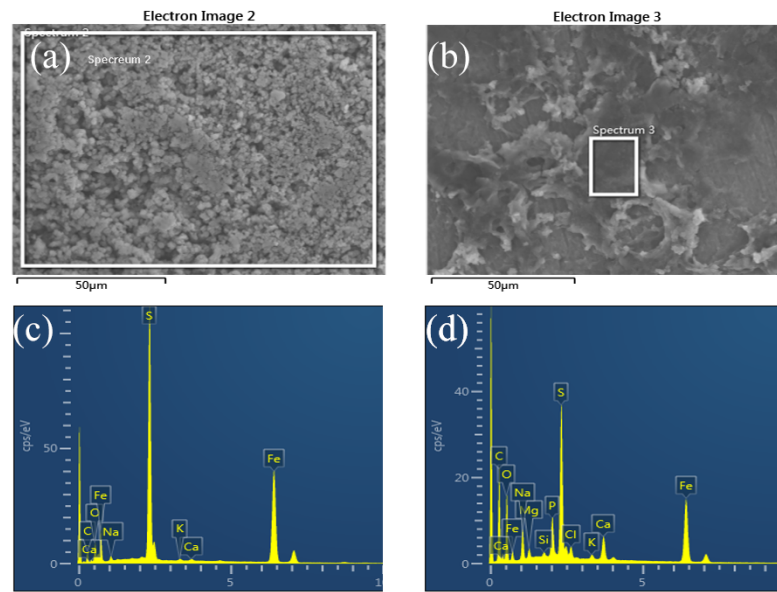


**Figure 2.** The morphologies and corresponding EDS spectra of (a,c) the cauliflower-like and (b,d) the network-like products of the Q235 steel after 7-day incubation in an SRB-Z-inoculated medium.

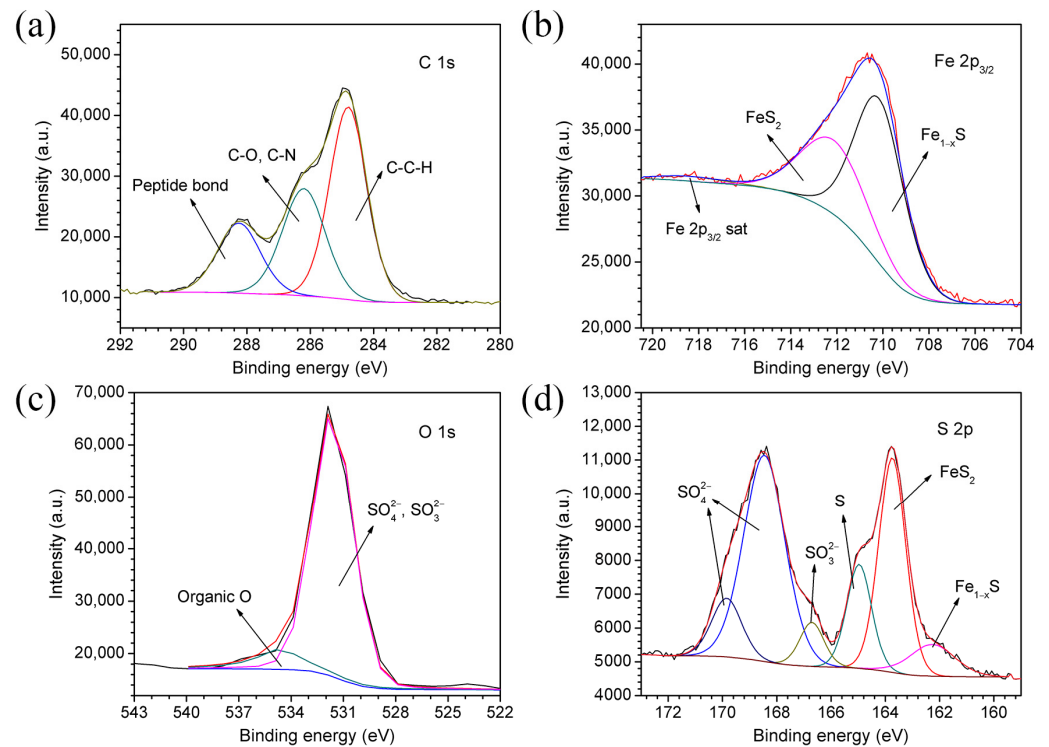


**Figure 3.** Chemical composition of the corrosion products after 7-day incubation in an SRB-Z-inoculated media. High resolution XPS spectra of (a) C 1s, (b) Fe 2p, (c) O 1s, and (d) S 2p.

### 3.2. Pit Morphology and Pit Depth

The morphology of pits on the coupon surface was examined using a 3D profilometer. Figure 4a shows the photograph and 3D profiles of the three deepest pits on the coupon surfaces. The pits did not resemble a pinhole. Macroscopically, the pits were shallow and broad, following the phenomenon as reported [43]. Microscopically, there were some deep pinholes in the bottom of the pits, which resembled the typical morphology of vertical grain corrosion. The length and depth of the pits were measured, as shown in Figure 4b–d. The maximum pit depth after incubation for 7 days in the SRB-Z-inoculated media reached

as deep as 42–54  $\mu\text{m}$ . The weight-loss test was also carried out, and the weight change of the Q235 carbon steel substrate was negligible.

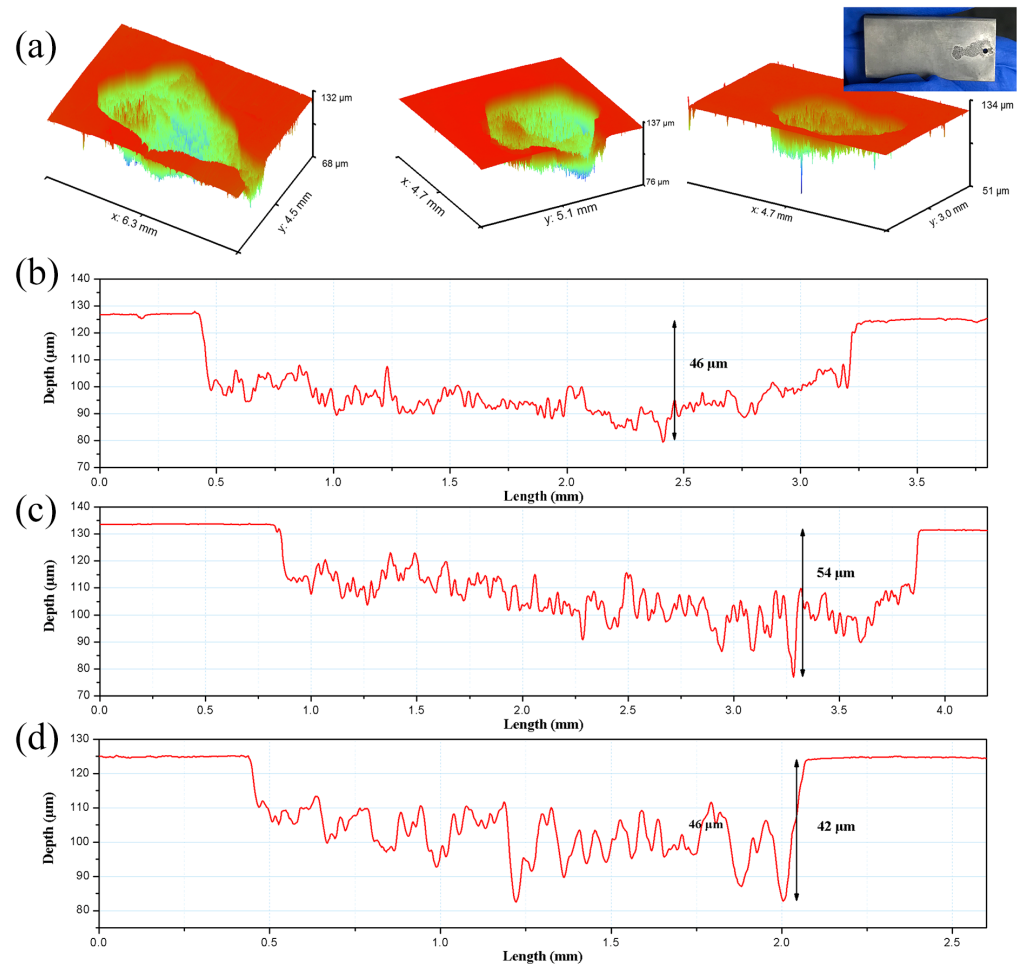


**Figure 4.** (a) 3D morphologies of the corrosion pits and (b–d) pits depth of the Q235 coupon after immersion corrosion test in SRB-Z solution for 7 days.

### 3.3. Electrochemical Measurements

The potentiodynamic polarization curves of the coupons immersed in sterile and SRB-Z-inoculated media after 7 days of incubation were both recorded (Figure 5). There is an obvious passivation zone in the polarization curve of the coupon immersed in the SRB-Z-inoculated medium. The corresponding electrochemical parameters are listed in Table 3. The Tafel slope is correlated with the rate of electrode reaction. A smaller value of the Tafel slope is indicative of the easier electron transference [44,45]. In the SRB-Z-inoculated medium, the anode Tafel slope  $\beta_a$  of the coupon is larger, and the cathodic Tafel slopes  $\beta_c$  of the coupon is smaller than that of the coupon incubated in a sterile medium, indicating that the anode reaction of the Q235 coupon was inhibited, but the cathodic reaction of the Q235 coupon was promoted. The corrosion potential,  $E_{corr}$ , undergoes a negative shift in the SRB-Z-inoculated medium, indicating that the thermodynamic corrosion tendency of the Q235 increased by the SRB-Z. The corrosion current densities  $I_{corr}$  of the coupon in the SRB-Z-inoculated medium were slightly larger than that of the coupon in the sterile medium. The data of  $I_{corr}$  indicate that the corrosion rate of the coupon accelerated by the SRB-Z on the 7th day.

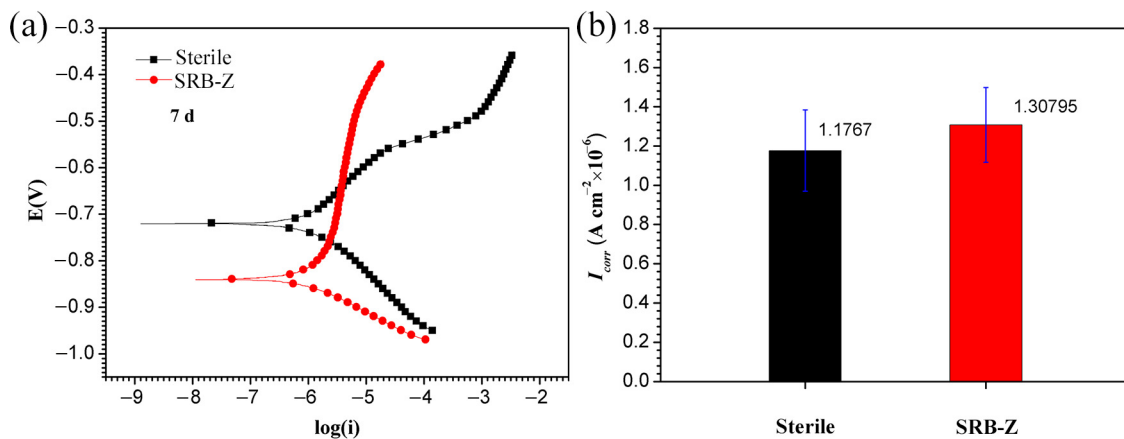


**Figure 5.** (a) Potentiodynamic polarization curves and (b)  $I_{corr}$  values and standard deviation values of the Q235 on the 7th day in the sterile media and the SRB-Z-inoculated media.

**Table 3.** Fitted parameters of potentiodynamic polarization curves of coupons in sterile and SRB-Z-inoculated media.

| Condition  | $\beta_a$<br>(V dec <sup>-1</sup> ) | $\beta_c$<br>(V dec <sup>-1</sup> ) | $E_{corr}$<br>(V vs. Ag/AgCl) | $I_{corr}$<br>(A cm <sup>-2</sup> ) |
|------------|-------------------------------------|-------------------------------------|-------------------------------|-------------------------------------|
| none-SRB-Z | 0.122                               | -0.109                              | -0.721                        | $1.03 \times 10^{-6}$               |
| SRB-Z      | 0.426                               | -0.077                              | -0.840                        | $1.44 \times 10^{-6}$               |

EIS is a non-destructive electrochemical technique for the characterization of electrochemical reactions at the metal/biofilm interface and formation of corrosion products and biofilms [46–50]. EIS data of the Q235 coupons were measured under stable OCP on the 1st, 4th, 7th, and 14th days. The impedance spectra are shown in Figure 6. Under sterile conditions (Figure 6a), the diameter of the impedance loop at a low frequency increases with time, reaching the maximum value on the fourteenth day, which reveals that the reaction resistance of the Q235 steel in the sterile medium increased with time. The Bode phase angle plot shows that the maximum angle broadened and shifted to a low frequency with time. Under the SRB-Z-inoculated conditions, the Nyquist plot of Q235 (Figure 6b) shows that the diameter of the impedance loop at low frequency increased sharply after the first day of incubation, which reveals that the reaction resistance of the Q235 steel was affected heavily by the SRB-Z. The Bode phase angle plot shows that the maximum phase angle did not shift but broadened from the 2nd day to the 14th day. The impedance magnitudes of the coupon in SRB-Z-inoculated media are much larger than that in the sterile media, indicating that the presence of SRB-Z reduced the uniform corrosion rate of Q235.

The impedance spectra of the Q235 coupons in sterile and SRB-Z-inoculated media with different immersion periods were analyzed and fitted to equivalent circuits. The two-time constant equivalent circuits were used, as shown in Figure 6e,f. The equivalent circuit A in Figure 6e is frequently used to represent a thin layer of product absorbed or deposited on the metal surface [46,49]. The Equivalent circuit B in Figure 6f is frequently used to represent a compact protective passivating film formed on the metal surface [44]. In the equivalent circuits,  $R_s$  represents the solution resistance;  $Q_f$  represents the constant phase element (CPE) of the biofilm or the corrosion product film on the Q235;  $R_f$  represents the resistance of the biofilm or the corrosion product film;  $Q_{dl}$  represents the CPE of the electrical double layer (EDL);  $R_{ct}$  corresponds to the charge transfer resistance at the interface of the coupon and the mixture of corrosion product and biofilm. According to the analysis of the polarization curve, the equivalent circuits A and B corresponded to the impedance spectra of Q235 steel exposed in sterile and SRB-Z-inoculated media, respectively. The parameters used for fitting are listed in Table 4. The value of  $R_f + R_{ct}$

is closely related to the corrosion rate; a higher value for a lower corrosion rate. Table 4 shows that  $R_{ct}$  was much larger than  $R_f$ ; Thus, the corrosion rate could be judged by  $R_{ct}$  alone. For the sterile group, the values of  $R_{ct}$  and  $Q_{dl}$  both increased with time, indicating that the charge transfer rate decreased during the 14 days of incubation, and is coincidental with the corrosion law of metal in an anaerobic environment. For the SRB-Z-inoculated group, the value of  $R_{ct}$  was much larger than that of the sterile group and increased with time, indicating that the density of the protective film increased with time. On the 14th day,  $R_{ct}$  decreased slightly, suggesting that the reaction product broke down or the pitting corrosion was induced by the SRB-Z.

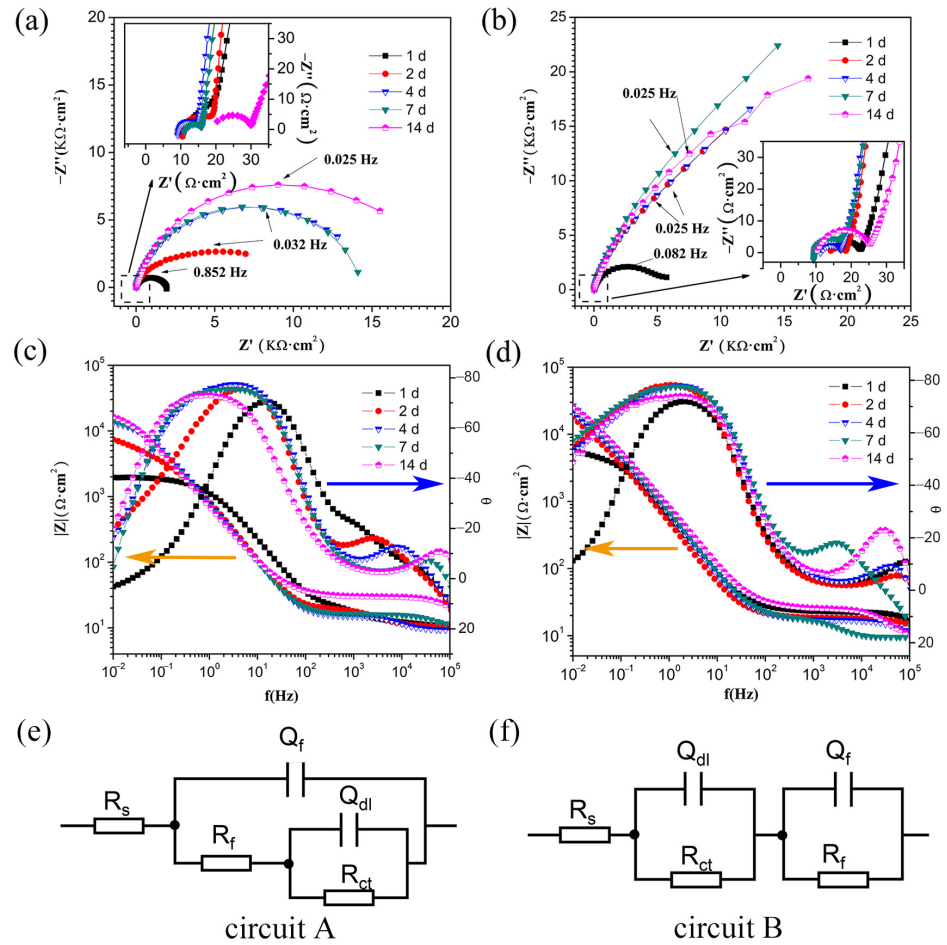


**Figure 6.** Nyquist and Bode plots for the Q235 in (a,c) the sterile media and (b,d) the SRB-Z-inoculated media, and (e,f) equivalent circuits used for fitting the EIS spectra of Q235.

**Table 4.** Fitted parameters of EIS.

| Condition        | $t$ (d) | $Q_f$<br>(kΩ <sup>-1</sup> s <sup>n</sup> cm <sup>-2</sup> ) | $R_f$<br>(Ω cm <sup>2</sup> ) | $Q_{dl}$<br>(kΩ <sup>-1</sup> s <sup>n</sup> cm <sup>-2</sup> ) | $R_{ct}$<br>(kΩ cm <sup>2</sup> ) |
|------------------|---------|--|-------------------------------|---|-----------------------------------|
| Sterile          | 1       | 95.60  | 21.90                         | 32.80   | 1.89                              |
|                  | 2       | 7.98   | 7.63                          | 259.00  | 6.71                              |
|                  | 4       | 4.77   | 5.18                          | 239.13  | 13.86                             |
|                  | 7       | 1.67   | 3.74                          | 249.77  | 14.19                             |
|                  | 14      | 0.59   | 10.32                         | 284.81  | 19.16                             |
| SRB-Z-inoculated | 1       | 1.91   | 8.92                          | 331.07  | 5.50                              |
|                  | 2       | 1.62   | 3.38                          | 425.77  | 32.08                             |
|                  | 4       | 1.12   | 4.87                          | 334.18  | 35.55                             |
|                  | 7       | 9.81   | 7.39                          | 301.29  | 55.32                             |
|                  | 14      | 0.63   | 14.12                         | 270.15  | 47.99                             |

#### 4. Discussion

In this study, the strain SRB-Z was isolated from the Pearl River and is a type of sulfate-reducing bacterium which can reduce the sulfate to hydrogen sulfide ( $H_2S$ ) [50]. The study results revealed that, in an anaerobic environment, the coupon immersed in the sterile medium corroded slightly and uniformly, and the uniform depth corrosion rate in the sterile system was much slower than the pitting rate incurred by SRB-Z. The SEM results displayed the morphologies of the SRB-Z cells and the corrosion products on the Q235 coupon surface, as shown in Figure 1e,f. The corrosion products were loose and thick in some regions and could be easily peeled off from the coupon surface even by the fluid shear. These corrosion products have a cauliflower-like morphology and a lamella shape on their top surface (Figure 1e). These lamellas grew along the vertical direction of the substrate, which is the typical morphology of mackinawite  $FeS$  [14,16,17]. The EDS mapping test results displayed that the concentration of Fe was higher in this region than in others, which suggests that abundant  $Fe^{2+}$  was passing through the loose corrosion product and was transported to the surface. Nevertheless, the  $Fe^{2+}$  could only possibly come from the continuous dissolution of the Q235 coupon substrate. As evidence, under the cauliflower-like product, the Q235 coupon showed a distinct bulgy grain boundary (Figure 1g), indicating that serious corrosion occurred on the coupons. The process described above explains why the corrosion pits usually appear under the thick and loose corrosion product. In other regions, the corrosion product was compact and thin. The corrosion product was difficult to brush clean with water. It reacted with acid and produced a rotten egg smell. The elemental test results revealed that the main composition was iron sulfide. All these phenomena indicated that the corrosion product might be incurred by the biogenic  $H_2S$ , which reacted with the metal ions and formed a protective  $FeS_x$  film on the metal surface. As reported, the initial  $FeS_x$  film was uniform and adhered tightly to the substrate. It could inhibit the corrosion of the substrate [51–53]. Thus, the existence of the biofilm restricted the growth and the shedding of  $FeS_x$  film to make it with continuous protection capability. Finally,  $FeS_x$  and the mineralized biofilm formed a layer of compounds that protected the metal from corrosion. This process explained why the Q235 substrate was corroded uniformly in this region. The corrosion processes in both regions were the interaction of SRB-Z cells, biofilm, iron ions, and biogenic  $H_2S$ . The value of impedance and corrosion current obtained from the EIS and the potentiodynamic polarization test are the average impedance and corrosion current values of the whole electrode plane. Due to most areas of the Q235 steel being covered by the protective compounds, the localized electrochemical behavior might be masked by the large area electrochemical behavior. Thus, the EIS results and polarization curves did not reveal the pitting corrosion of Q235 steel in the SRB-Z-inoculated medium but revealed that the compounds comprising SRB-Z biofilm and  $FeS_x$  on the coupon surface protected the coupon from uniform corrosion. According to the existing mechanisms, the promoted cathodic reaction suggests that the extracellular electron transfer [54] process might be promoted by the SRB-Z.

Two types of composition and morphology must correspond to two distinct corrosion processes. The SRB-Z influenced the pitting corrosion process, and the mechanism of Q235 carbon steel was proposed according to the test results; the process is illustrated in Figure 7. First, the SRB-Z adhered and formed biofilm on the Q235 coupon surface. The amount of  $H_2S$  in the medium was much less. Second, with the growth of SRB-Z, a large amount of  $H_2S$  was produced by SRB-Z [32]. In the sealing system, the concentration of  $H_2S$  reached  $39 \text{ mmol L}^{-1}$ . The medium was acidized. The biogenic  $H_2S$  penetrated the biofilm and reacted with the Q235 steel. The reaction rate was restricted by the barrier function of the biofilm, thus the formed  $FeS_x$  layer was compact and protective. Third, due to the heterogeneity of the biofilm, in local regions, the biofilm was thick; with the biofilm developed to the mature period, the biofilm fell off, and the fresh steel surface was exposed to the  $H_2S$  environment. The fresh steel surface acted as a small anode. The region covered by the compounds composed of  $FeS_x$  and the SRB-Z biofilm acted as a large cathode, causing  $FeS$ -SRB/Fe galvanic corrosion. Then the exposed fresh Q235 steel

dissolved quickly. Finally, a large amount of Fe ions were produced in local regions. They reacted with  $H_2S$  rapidly, resulting in loose and thick reaction products above the exposed fresh surface. The loose  $FeS_x$  easily broke down from the surface of the coupon and could not resist corrosion. Then the pitting corrosion occurred.

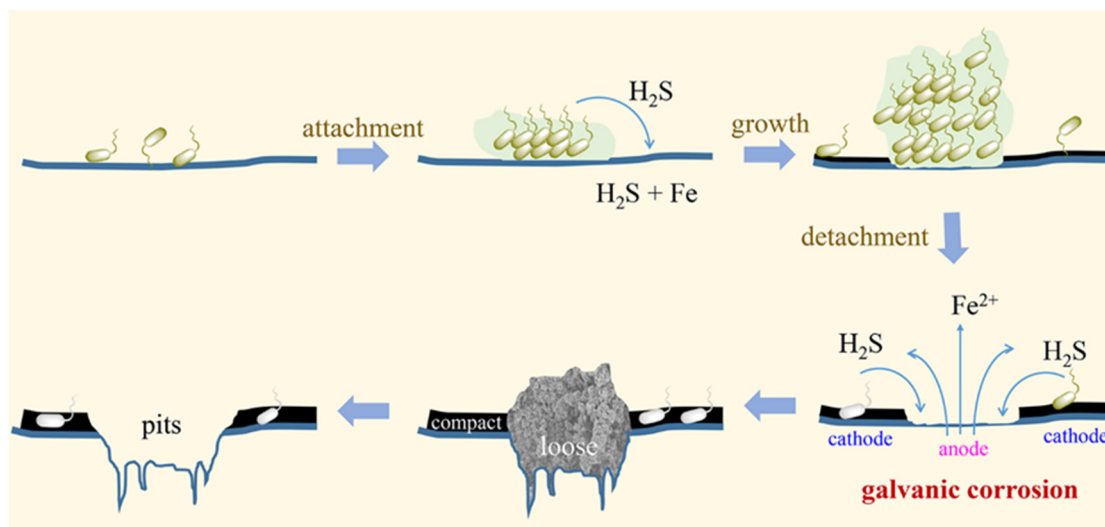


**Figure 7.** Schematic illustration of the corrosion behavior and mechanism of Q235 under the SRB-Z condition.

In nature, bacteria tend to adhere to objects and form a biofilm [55]. Therefore, metals buried in soil or immersed in water will have SRB assembled on their surface, thus forming a local  $H_2S$  and SRB environment. Pitting corrosion will occur according to the process described in this work. Nevertheless, the real application of these experiments will be time consuming and should be carried out. In the future, more environmentally relevant data should be provided to make the simulated environment closer to the natural environment [5]. The study of MIC has significant prospects.

## 5. Conclusions

In conclusion, a strain belonging to *Desulfovibrio* sp. named SRB-Z was isolated from the Pearl River in Guangzhou, and the effect of SRB-Z on the corrosion behavior and mechanism of Q235 carbon steel was investigated. The results of these investigations are as follows:

- (1) The isolated SRB-Z could induce severe pitting corrosion of Q235. The pit depth reached about  $54\ \mu m$  within a week.
- (2) The distribution of reaction products, biofilm, and bacteria is heterogeneous on the coupon surface.  $FeS_x$  was found as the main reaction product. Over the corrosion pits, the product was cauliflower-like, thick, loose, and with little SRB-Z and mainly composed of  $FeS_x$ . Over the uniform corrosion area, the product had a network-like morphology comprising biofilm and bacteria.
- (3) The corrosion risk and rate of Q235 were both elevated because the cathode reaction was accelerated by SRB-Z. The formation of the  $FeS$ -SRB/Fe galvanic couple incurred localized corrosion on the Q235 coupon surfaces.

**Author Contributions:** H.Q.: Conceptualization, Data curation, Writing—Original draft. Q.S.: Project administration, Writing—Review & Editing. R.P.: Methodology. T.S.: Methodology, Investigation. Z.Z.: Funding acquisition. L.L.: Supervision. X.X.: Supervision, Funding acquisition. All authors have read and agreed to the published version of the manuscript.

**Funding:** This research was funded by the GDAS' Project of Science and Technology Development, grant number 2019GDASYL-0103014; the Guangdong Provincial Key Laboratory of Electronic Information Products Reliability Technology, grant number 2017B030314151; the Science and Technology Planning Project of Guangzhou, grant number 202201010124.

**Institutional Review Board Statement:** Not applicable.

**Informed Consent Statement:** Not applicable.

**Data Availability Statement:** The raw/processed data required to reproduce these findings cannot be shared at this time due to technical or time limitations.

**Conflicts of Interest:** The authors declare no conflict of interest.

## References

1. Lou, Y.; Chang, W.; Cui, T.; Wang, J.; Qian, H.; Ma, L.; Hao, X.; Zhang, D. Microbiologically influenced corrosion inhibition mechanisms in corrosion protection: A review. *Bioelectrochemistry* **2021**, *141*, 107883. [[CrossRef](#)] [[PubMed](#)]
2. Jia, R.; Unsal, T.; Xu, D.; Leckbach, Y.; Gu, T. Microbiologically influenced corrosion and current mitigation strategies: A state of the art review. *Int. Biodeter. Biodegr.* **2019**, *137*, 42–58. [[CrossRef](#)]
3. Zhou, E.; Li, F.; Zhang, D.; Xu, D.; Li, Z.; Jia, R.; Jin, Y.; Song, H.; Li, H.; Wang, Q.; et al. Direct microbial electron uptake as a mechanism for stainless steel corrosion in aerobic environments. *Water Res.* **2022**, *219*, 118553. [[CrossRef](#)] [[PubMed](#)]
4. Little, B.J.; Blackwood, D.J.; Hinks, J.; Lauro, F.M.; Marsili, E.; Okamoto, A.; Rice, S.A.; Wade, S.A.; Flemming, H.C. Microbially influenced corrosion—Any progress? *Corros. Sci.* **2020**, *170*, 108641. [[CrossRef](#)]
5. Vigneron, A.; Head, I.M.; Tsesmetzis, N. Damage to offshore production facilities by corrosive microbial biofilms. *Appl. Microb. Biotech.* **2018**, *102*, 2525–2533. [[CrossRef](#)]
6. Vigneron, A.; Alsop, E.B.; Chambers, B.; Lomans, B.P.; Head, I.M.; Tsesmetzis, N. Complementary microorganisms in highly corrosive biofilms from an offshore oil production facility. *Appl. Environ. Microb.* **2016**, *82*, 2545–2554. [[CrossRef](#)]
7. Wu, T.; Yan, M.; Yu, L.; Zhao, H.; Sun, C.; Yin, F.; Ke, W. Stress corrosion of pipeline steel under disbanded coating in a SRB-containing environment. *Corros. Sci.* **2019**, *157*, 518–530. [[CrossRef](#)]
8. Wu, T.; Sun, C.; Ke, W. Interpreting microbiologically assisted cracking with E(e)-pH diagrams. *Bioelectrochemistry* **2018**, *120*, 57–65. [[CrossRef](#)]
9. Wu, T.; Yan, M.; Zeng, D.; Xu, J.; Sun, C.; Yu, C.; Ke, W. Stress corrosion cracking of X80 steel in the presence of sulfate-reducing bacteria. *J. Mater. Sci. Technol.* **2015**, *31*, 413–422. [[CrossRef](#)]
10. Wu, T.; Xu, J.; Yan, M.; Sun, C.; Yu, C.; Ke, W. Synergistic effect of sulfate-reducing bacteria and elastic stress on corrosion of X80 steel in soil solution. *Corros. Sci.* **2014**, *83*, 38–47. [[CrossRef](#)]
11. Zhang, T.; Wang, J.; Li, G.; Liu, H. Crevice corrosion of X80 carbon steel induced by sulfate reducing bacteria in simulated seawater. *Bioelectrochemistry* **2021**, *142*, 107933. [[CrossRef](#)] [[PubMed](#)]
12. Dou, W.; Liu, J.; Cai, W.; Wang, D.; Jia, R.; Chen, S.; Gu, T. Electrochemical investigation of increased carbon steel corrosion via extracellular electron transfer by a sulfate reducing bacterium under carbon source starvation. *Corros. Sci.* **2019**, *150*, 258–267. [[CrossRef](#)]
13. Li, Y.; Feng, S.; Liu, H.; Tian, X.; Xia, Y.; Li, M.; Xu, K.; Yu, H.; Liu, Q.; Chen, C. Bacterial distribution in SRB biofilm affects MIC pitting of carbon steel studied using FIB-SEM. *Corros. Sci.* **2020**, *167*, 108512. [[CrossRef](#)]
14. Wang, D.; Kijjka, P.; Mohamed, M.E.; Saleh, M.A.; Kumseranee, S.; Punpruk, S.; Gu, T. Aggressive corrosion of carbon steel by *Desulfovibrio ferrophilus* IS5 biofilm was further accelerated by riboflavin. *Bioelectrochemistry* **2021**, *142*, 107920. [[CrossRef](#)] [[PubMed](#)]
15. Liang, Y.; Li, C.; Wang, P.; Zhang, D. Fabrication of a robust slippery liquid infused porous surface on Q235 carbon steel for inhibiting microbiologically influenced corrosion. *Colloid. Surface A Physicochem. Eng. Asp.* **2021**, *631*, 127696. [[CrossRef](#)]
16. Guan, F.; Duan, J.; Zhai, X.; Wang, N.; Zhang, J.; Lu, D.; Hou, B. Interaction between sulfate-reducing bacteria and aluminum alloys—Corrosion mechanisms of 5052 and Al-Zn-In-Cd aluminum alloys. *J. Mater. Sci. Technol.* **2020**, *36*, 55–64. [[CrossRef](#)]
17. Gu, T.; Wang, D.; Leckbach, Y.; Xu, D. Extracellular electron transfer in microbial biocorrosion. *Curr. Opin. Electrochem.* **2021**, *29*, 100763. [[CrossRef](#)]
18. Wei, B.; Xu, J.; Cheng, Y.F.; Sun, C.; Yu, C.; Wang, Z. Effect of uniaxial elastic stress on corrosion of X80 pipeline steel in an acidic soil solution containing sulfate-reducing bacteria trapped under disbanded coating. *Corros. Sci.* **2021**, *193*, 109893. [[CrossRef](#)]
19. Davidova, I.A.; Lenhart, T.R.; Nanny, M.A.; Sufliata, J.M. Composition and corrosivity of extracellular polymeric substances from the hydrocarbon-degrading sulfate-reducing bacterium *Desulfohalobium alkaexedens* ALDC. *Microorganisms* **2021**, *9*, 1994. [[CrossRef](#)]
20. Wang, D.; Yang, C.; Saleh, M.A.; Alotaibi, M.D.; Mohamed, M.E. Conductive magnetite nanoparticles considerably accelerated carbon steel corrosion by electroactive *Desulfovibrio vulgaris* biofilm. *Corros. Sci.* **2022**, *205*, 110440. [[CrossRef](#)]
21. Lan, X.; Zhang, J.; Wang, Z.; Zhang, R.; Sand, W.; Zhang, L.; Duan, J.; Zhu, Q.; Hou, B. Corrosion of an AZ31B magnesium alloy by sulfate-reducing prokaryotes in a mudflat environment. *Microorganisms* **2022**, *10*, 839. [[CrossRef](#)] [[PubMed](#)]

22. Salgar-Chaparro, S.J.; Lepkova, K.; Pojtanabuntoeng, T.; Darwin, A.; Machuca, L.L. Microbiologically influenced corrosion as a function of environmental conditions: A laboratory study using oilfield multispecies biofilms. *Corros. Sci.* **2020**, *169*, 108595. [[CrossRef](#)]
23. Sharma, M.; Liu, H.; Tsesmetzis, N.; Handy, J.; Place, T.; Gieg, L.M. Diagnosing microbiologically influenced corrosion at a crude oil pipeline facility leak site—A multiple lines of evidence approach. *Int. Biodeter. Biodegr.* **2022**, *172*, 105438. [[CrossRef](#)]
24. Li, Y.; Xu, D.; Chen, C.; Li, X.; Ru, J.; Zhang, D.; Sand, W.; Wang, F.; Gu, T. Anaerobic microbiologically influenced corrosion mechanisms interpreted using bioenergetics and bioelectrochemistry: A review. *J. Mater. Sci. Technol.* **2018**, *34*, 1713–1718. [[CrossRef](#)]
25. Venzlaff, H.; Enning, D.; Srinivasan, J.; Mayrhofer, K.J.J.; Hassel, A.W.; Widdel, F.; Stratmann, M. Accelerated cathodic reaction in microbial corrosion of iron due to direct electron uptake by sulfate-reducing bacteria. *Corros. Sci.* **2013**, *66*, 88–96. [[CrossRef](#)]
26. Biofilms, I.B.; Sztyler, M.; Gaylarde, C.C.; Smith, W.L.; Sunner, J. *Biofilms and Biocorrosion*; Woodhead Publishing Limited: Cambridge, UK, 2014.
27. Lappin-Scott, H.; Burton, S.; Stoodley, P. Revealing a world of biofilms—the pioneering research of Bill Costerton. *Nat. Rev. Microbiol.* **2014**, *12*, 781–787. [[CrossRef](#)] [[PubMed](#)]
28. Hall-Stoodley, L.; Costerton, J.W.; Stoodley, P. Bacterial biofilms: From the natural environment to infectious diseases. *Nat. Rev. Microbiol.* **2004**, *2*, 95–108. [[CrossRef](#)]
29. Dong, Z.H.; Shi, W.; Ruan, H.M.; Zhang, G.A. Heterogeneous corrosion of mild steel under SRB-biofilm characterised by electrochemical mapping technique. *Corr. Sci.* **2011**, *53*, 2978–2987. [[CrossRef](#)]
30. Liu, H.; Cheng, Y.F. Microbial corrosion of X52 pipeline steel under soil with varied thicknesses soaked with a simulated soil solution containing sulfate-reducing bacteria and the associated galvanic coupling effect. *Electrochim. Acta* **2018**, *266*, 312–325. [[CrossRef](#)]
31. Enning, D.; Garrelfs, J. Corrosion of iron by sulfate-reducing bacteria: New views of an old problem. *Appl. Environ. Microbiol.* **2014**, *80*, 1226–1236. [[CrossRef](#)]
32. Shi, F.; Zhang, L.; Yang, J.; Lu, M.; Ding, J.; Li, H. Polymorphous FeS corrosion products of pipeline steel under highly sour conditions. *Corros. Sci.* **2016**, *102*, 103–113. [[CrossRef](#)]
33. Dong, Y.; Song, G.L.; Zheng, D. Naturally effective inhibition of microbial corrosion by bacterium-alga symbiosis on 304 stainless steel. *J. Clean. Prod.* **2022**, *356*, 131823. [[CrossRef](#)]
34. Wei, H.; Yang, X.Y.; van der Mei, H.C.; Busscher, H.J. X-ray photoelectron spectroscopy on microbial cell surfaces: A forgotten method for the characterization of microorganisms encapsulated with surface-engineered shells. *Front. Chem.* **2021**, *9*, 666159. [[CrossRef](#)] [[PubMed](#)]
35. Kjaervik, M.; Ramstedt, M.; Schwibbert, K.; Dietrich, P.M.; Unger, W.E.S. Comparative study of NAP-XPS and Cryo-XPS for the investigation of surface chemistry of the bacterial cell-envelope. *Front. Chem.* **2021**, *9*, 666161. [[CrossRef](#)] [[PubMed](#)]
36. Briggs, D. *Handbook of X-ray Photoelectron Spectroscopy*, 3rd ed.; Perkin-Elmer Corp., Physical Electronics Division: Eden Prairie, MN, USA, 1979; p. 81.
37. Shah, M.; Ayob, M.T.M.; Rosdan, R.; Yaakob, N.; Embong, Z.; Othman, N.K. The effect of H<sub>2</sub>S pressure on the formation of multiple corrosion products on 316L stainless steel surface. *Sci. World J.* **2020**, *2020*, 3989563. [[CrossRef](#)]
38. Kobayashi, Y.; Fujiwara, Y. Effect of SO<sub>4</sub><sup>2-</sup> on the corrosion behavior of cerium-based conversion coatings on galvanized steel. *Electrochim. Acta.* **2006**, *51*, 4236–4242. [[CrossRef](#)]
39. Katan, T.; Kargl, R.; Mohan, T.; Steindorfer, T.; Mozetič, M.; Kovač, J.; Kleinschek, K.S. Solid phase peptide synthesis on chitosan thin films. *Biomacromolecules* **2022**, *23*, 731–742. [[CrossRef](#)]
40. Cha, B.J.; Choi, J.Y.; Ji, Y.; Zhao, S.; Kima, S.Y.; Kima, S.H.; Kima, Y.D. Fe-oxide/Al<sub>2</sub>O<sub>3</sub> for the enhanced activity of H<sub>2</sub>S decomposition under realistic conditions: Mechanistic studies by in-situ DRIFTS and XPS. *Chem. Eng. J.* **2022**, *443*, 136459. [[CrossRef](#)]
41. Liao, K.; Leng, J.; Cheng, Y.F.; He, T.; He, G.; Zhao, S.; Liu, X.; Huang, Q. Effect of H<sub>2</sub>S concentrations on corrosion failure of L245NS steel in CO<sub>2</sub>-O<sub>2</sub>-H<sub>2</sub>S system. *Process. Saf. Environ.* **2022**, *168*, 224–238. [[CrossRef](#)]
42. Xu, H.; Wang, T.; Koppala, S.; Hu, J.; Ma, S.; Miao, W.; Le, T.; Zhang, L. Improving the quality of ammonium sulfate produced from the flue gas desulfurization process by using ammonium persulfate. *Sep. Purif. Technol.* **2023**, *308*, 122879. [[CrossRef](#)]
43. Duret-Thual, C. Understanding corrosion: Basic principles. In *Understanding Biocorrosion*, 1st ed.; Liengen, T., Beech, I.B., Eds.; Woodhead Publishing Limited: Cambridge, UK, 2014; Volume 1, pp. 3–32.
44. Yuan, S.J.; Pehkonen, S.O.; Ting, Y.P.; Kang, E.T.; Neoh, K.G. Corrosion behavior of type 304 stainless steel in a simulated seawater-based medium in the presence and absence of aerobic *Pseudomonas* NCIMB 2021 bacteria. *Ind. Eng. Chem. Res.* **2008**, *47*, 3008–3020. [[CrossRef](#)]
45. Huang, G.; Chan, K.Y.; Fang, H.H.P. Microbiologically induced corrosion of 70Cu-30Ni alloy in anaerobic seawater. *J. Electrochem. Soc.* **2004**, *151*, B434. [[CrossRef](#)]
46. Ru, J.; Yang, D.; Xu, J.; Xu, D.; Gu, T. Microbiologically influenced corrosion of C1018 carbon steel by nitrate reducing *Pseudomonas aeruginosa* biofilm under organic carbon starvation. *Corros. Sci.* **2017**, *127*, 1–9.
47. Cetin, D.; Aksu, M.L. Corrosion behavior of low-alloy steel in the presence of *Desulfotomaculum* sp. *Corros. Sci.* **2009**, *51*, 1584–1588. [[CrossRef](#)]

48. Belkaid, S.; Ladjouzi, M.A.; Hamdani, S. Effect of biofilm on naval steel corrosion in natural seawater. *J. Solid State Electrochem.* **2011**, *15*, 525–537. [[CrossRef](#)]
49. Fu, C.; Gu, T.; Zhang, G.; Lv, Y.; Wang, H.; Liu, H. Corrosion behavior of carbon steel in the presence of sulfate reducing bacteria and iron oxidizing bacteria cultured in oilfield produced water. *Corros. Sci.* **2015**, *100*, 484–495.
50. Nicoletti, D.; Sharma, M.; Gieg, L.M. Assessing microbial corrosion risk on offshore crude oil production topsides under conditions of nitrate and nitrite treatment for souring. *Microorganisms* **2022**, *10*, 932. [[CrossRef](#)] [[PubMed](#)]
51. Bai, P.; Zhao, H.; Zheng, S.; Chen, C. Initiation and developmental stages of steel corrosion in wet H<sub>2</sub>S environments. *Corros. Sci.* **2015**, *93*, 109–119. [[CrossRef](#)]
52. Ma, H.; Cheng, X.; Li, G.; Chen, S.; Quan, Z.; Zhao, S.; Niu, L. The influence of hydrogen sulfide on corrosion of iron under different conditions. *Corr. Sci.* **2000**, *42*, 1669–1683. [[CrossRef](#)]
53. Tang, J.; Shao, Y.; Guo, J.; Zhang, T.; Meng, G.; Wang, F. The effect of H<sub>2</sub>S concentration on the corrosion behavior of carbon steel at 90 °C. *Corr. Sci.* **2010**, *52*, 2050–2058. [[CrossRef](#)]
54. Beese-Vasbender, P.F.; Nayak, S.; Erbe, A.; Stratmann, M.; Mayrhofer, K.J.J. Electrochemical characterization of direct electron uptake in electrical microbially influenced corrosion of iron by the lithoautotrophic SRB *Desulfopila corrodens* strain IS4. *Electrochim. Acta.* **2015**, *167*, 321–329. [[CrossRef](#)]
55. Aktas, D.F.; Sorrell, K.R.; Duncan, K.E.; Wawrik, B.; Callaghan, A.V.; Sufliya, J.M. Anaerobic hydrocarbon biodegradation and biocorrosion of carbon steel in marine environments: The impact of different ultralow sulfur diesels and bioaugmentation. *Int. Biodeterior. Biodegrad.* **2017**, *118*, 45–56. [[CrossRef](#)]

**Disclaimer/Publisher’s Note:** The statements, opinions and data contained in all publications are solely those of the individual author(s) and contributor(s) and not of MDPI and/or the editor(s). MDPI and/or the editor(s) disclaim responsibility for any injury to people or property resulting from any ideas, methods, instructions or products referred to in the content.